

Persistent spin dynamics in the Ising triangular-lattice antiferromagnet $\text{Ba}_6\text{Nd}_2\text{Ti}_4\text{O}_{17}$ C. Y. Jiang ¹, B. L. Chen,¹ K. W. Chen ¹, J. C. Jiao ¹, Y. Wang,¹ Q. Wu,¹ N. Y. Zhang,¹ M. Y. Zou,¹ Pei-Chun Ho ², Oscar O. Bernal ³, Douglas E. MacLaughlin,⁴ and Lei Shu ^{1,5,*}¹*State Key Laboratory of Surface Physics, Department of Physics, Fudan University, Shanghai 200438, China*²*Department of Physics, California State University, Fresno, California 93740, USA*³*Department of Physics and Astronomy, California State University, Los Angeles, California 90032, USA*⁴*Department of Physics and Astronomy, University of California, Riverside, California 92520, USA*⁵*Shanghai Research Center for Quantum Sciences, Shanghai 201315, China*

(Received 26 September 2024; revised 18 March 2025; accepted 14 April 2025; published 28 April 2025)

We report results of magnetic susceptibility, specific heat, and muon spin relaxation measurements on the polycrystalline titanate $\text{Ba}_6\text{Nd}_2\text{Ti}_4\text{O}_{17}$, an essentially disorder-free triangular-lattice antiferromagnet. The absence of long-range magnetic order or spin freezing is confirmed down to 30 mK, well below the Curie-Weiss temperature -1.8 K. Magnetism and specific heat measurements reveal Ising-like effective-spin-1/2 behavior. Persistent spin dynamics are observed down to 37 mK. Our study has discovered a remarkable example of Ising spins on the triangular lattice, which remains magnetically disordered at low temperatures and potentially hosts a quantum spin liquid ground state.

DOI: [10.1103/PhysRevB.111.155148](https://doi.org/10.1103/PhysRevB.111.155148)**I. INTRODUCTION**

A quantum spin liquid (QSL) is an exotic magnetic state, in which spins are highly entangled and remain disordered even in disorder-free lattices at zero temperature due to strong quantum fluctuations [1–4]. Beyond the traditional Landau symmetry breaking paradigm, QSL is characterized by fractionalized spin excitations instead of an order parameter [5,6]. The triangular-lattice antiferromagnet with isotropic Heisenberg interactions was proposed to host a QSL ground state by Anderson in the resonating valence bond picture [7], but a magnetically ordered ground state was subsequently demonstrated [8] even for a spin-1/2 system where the quantum effects are most significant. The magnetic order is fragile, however, and can be “melted” by other interactions, such as next-nearest-neighbor couplings [9,10], spatially anisotropic exchange interactions [11], or magnetic anisotropy [12,13]. These properties provide alternative ways to realize a QSL.

Rare-earth (RE)-based frustrated lattices represent promising habitats for QSL, since the strong atomic spin-orbit coupling (SOC) gives rise to both spatial and spin anisotropies [14,15]. YbMgGaO_4 and the chalcogenides family NaYbCh_2 ($Ch = \text{O}, \text{S}, \text{Se}$) have attracted much attention due to potential QSL properties [16–21]. SOC together with the crystal electric field (CEF) leads to a Kramers ground-state doublet characterized by an effective spin-1/2 in these magnets [14]. However, the effective spin exhibits easy-plane magnetic anisotropy for the RE-based triangular lattices that have been extensively studied so far.

The Nd-based triangular-lattice tantalate $\text{NdTa}_7\text{O}_{19}$ has recently been reported to be a potential QSL candidate [22]. In

it the effective spin-1/2 Nd^{3+} moments are Ising-like, giving rise to spin excitations down to 40 mK. As a triangular lattice with Ising spins, $\text{NdTa}_7\text{O}_{19}$ provides a promising system in which to realize QSL and other novel quantum states, which have not been studied before due to limited availability of materials [23]. An early theoretical study of the classical Ising model on a triangular lattice by Wannier [24] led to a classical spin-liquid state. Since then theoretical studies [25,26] have predicted exotic states of Ising spins on the triangular lattice. Synthesis and study of new Ising triangular-lattice materials are needed.

This paper reports comprehensive studies of magnetic susceptibility, specific heat, and muon spin relaxation (μSR) in polycrystalline $\text{Ba}_6\text{Nd}_2\text{Ti}_4\text{O}_{17}$, which is an essentially disorder-free Nd^{3+} triangular lattice. An Ising-like spin anisotropy is supported by magnetization and specific heat results, which complement a previous study [27]. The absence of magnetic order was confirmed down to 30 mK by zero-field (ZF) μSR measurements, despite a low-temperature Curie-Weiss (CW) temperature $\Theta_{\text{CW,L}} = -1.8$ K. A two-level Schottky anomaly was observed in the field dependence of the magnetic specific heat, indicating the spin is effectively 1/2 at low temperatures. The magnetically disordered state with effective spin-1/2 was further studied by longitudinal-field (LF) μSR measurements, which reveal persistent spin dynamics down to 37 mK. Our results provide strong evidence for a QSL in $\text{Ba}_6\text{Nd}_2\text{Ti}_4\text{O}_{17}$.

II. EXPERIMENT

Polycrystalline $\text{Ba}_6\text{Nd}_2\text{Ti}_4\text{O}_{17}$ was synthesized by the solid state reaction method [28]. The starting materials BaCO_3 , TiO_2 , Nd_2O_3 were first dried overnight at 700°C . Stoichiometric amounts of reagents were then mixed,

*Contact author: leishu@fudan.edu.cn

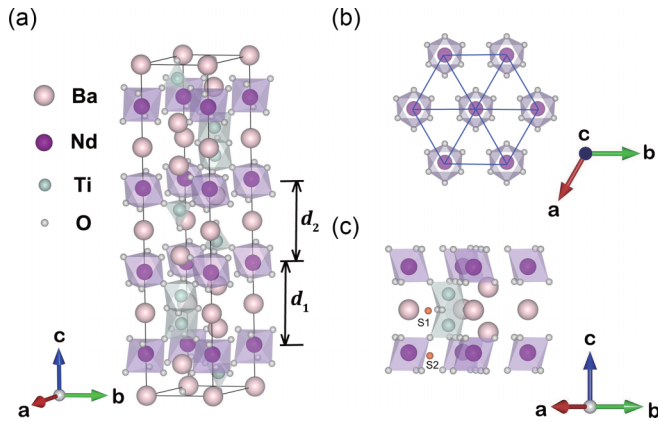


FIG. 1. (a) Unit cell of $\text{Ba}_6\text{Nd}_2\text{Ti}_4\text{O}_{17}$. (b) Top view of the triangular lattice formed by Nd^{3+} ions. (c) Orange spheres: two possible μ^+ stopping sites S1 and S2 (Sec. IV B).

thoroughly ground, and prereacted at 900°C for 12 h. The samples were finally reground and heated to 1250°C for 48 h in air, repeating 2–3 times. Powder x-ray diffraction (XRD) data were collected using a Bruker D8 advanced x-ray diffraction spectrometer ($\lambda = 1.5418 \text{ \AA}$) at room temperature. Structural refinements were performed using the FULLPROF software package [29].

The magnetization and dc magnetic susceptibility were measured using a Magnetic Property Measurement System (MPMS, Quantum Design). The specific heat measurements were performed by the adiabatic relaxation method in a Physical Property Measurement System (PPMS) (DynaCool, Quantum Design) equipped with a Helium-3 option. μSR measurements were carried out at TRIUMF, Vancouver, Canada, using the LAMPF spectrometer at the M20 beamline and the dilution refrigerator (DR) spectrometer at the M15 beamline. The samples were mounted on a silver holder in the DR spectrometer and encased in thin silver tape in the LAMPF spectrometer. The μSR data were analyzed using the MUSRFIT software package [30].

III. RESULTS

A. Structure

Polycrystalline $\text{Ba}_6\text{Nd}_2\text{Ti}_4\text{O}_{17}$ was synthesized in 2002 [28], and single crystals have been grown recently [27]. The crystal structure of $\text{Ba}_6\text{Nd}_2\text{Ti}_4\text{O}_{17}$ (space group $P6_3/mmc$) is shown in Fig. 1(a) (see Ref. [27] for details of the structure determination). The Nd^{3+} ions form triangular layers in the ab plane, as shown in Fig. 1(b). The layers are stacked along the c axis, and are separated by two different interlayer distances $d_1 = 7.40 \text{ \AA}$ and $d_2 = 7.56 \text{ \AA}$ due to different interlayer Ti coordinations. The geometry is such that spin exchange is strongest within Nd^{3+} layers, and superexchange between layers is considerably stronger across the shorter distance. The two possible positive-muon (μ^+) stopping sites S1 and S2 discussed in Sec. IV B are shown in Fig. 1(c). Site S1 is located between two Nd^{3+} layers, and S2 is in a Nd^{3+} layer.

Powder x-ray diffraction (XRD) measurements were performed on polycrystalline $\text{Ba}_6\text{Nd}_2\text{Ti}_4\text{O}_{17}$ to determine the sample quality. The XRD pattern and Rietveld refinements

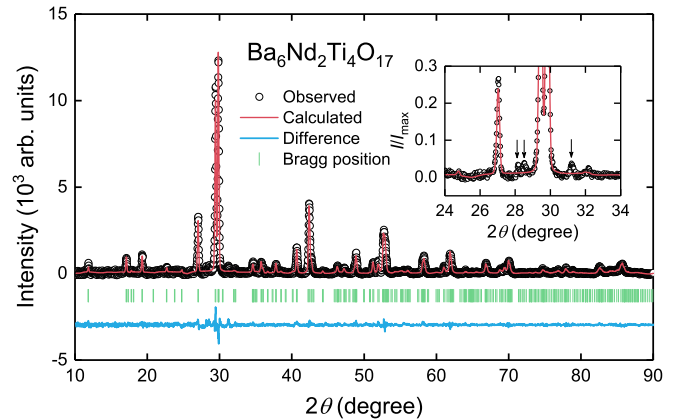


FIG. 2. XRD pattern and Rietveld refinement results for $\text{Ba}_6\text{Nd}_2\text{Ti}_4\text{O}_{17}$. Inset: enlarged view of the region $2\theta = 24^\circ\text{--}34^\circ$. Arrows: small peaks of unknown origin.

are shown in Fig. 2, and refinement parameters are listed in Table I. The results are essentially the same as previously reported [27], although the refinement exhibits three unexpected small peaks at $2\theta = 24^\circ\text{--}34^\circ$, shown in the inset of Fig. 2. None of the residual starting materials are matched by these peaks, and $\text{Nd}^{3+}/\text{Ba}^{2+}$ or $\text{Nd}^{3+}/\text{Ti}^{4+}$ site-mixing disorder is also not matched. The absence of site-mixing disorder was also reported for single crystal $\text{Ba}_6\text{Nd}_2\text{Ti}_4\text{O}_{17}$ [27]. The unexpected peaks may originate from dilute impurity phases with superlattice structures.

B. Magnetic properties

The temperature dependences of the dc magnetic susceptibility χ and inverse susceptibility χ^{-1} of $\text{Ba}_6\text{Nd}_2\text{Ti}_4\text{O}_{17}$ are shown in Fig. 3(a). The magnetic susceptibility was measured at 1 T with zero-field cooling (ZFC) and field cooling (FC). No sharp magnetic transition was observed down to 2 K and no obvious difference between ZFC and FC curves was detected, indicating the absence of spin ordering or freezing. A CW fit at high temperatures (100–200 K) yields an effective magnetic moment $\mu_{\text{eff,H}} = 3.43 \mu_B$, close to the Hund's-rules

TABLE I. Rietveld refinement results for $\text{Ba}_6\text{Nd}_2\text{Ti}_4\text{O}_{17}$ XRD data measured at room temperature. Cell parameters: $\alpha = \beta = 90^\circ$, $\gamma = 120^\circ$, $a = b = 5.9922(4) \text{ \AA}$, $c = 29.927(2) \text{ \AA}$. Overall $B = 0.33(6) \text{ \AA}^2$. The space group is $P6_3/mmc$. $\chi^2 = 2.40$.

Atom	Wyckoff position	x	y	z	Occ.
Nd	4e	0	0	0.1263(2)	1
Ba1	2a	0	0	0	1
Ba2	4f	0.6667	0.3333	0.0861(3)	1
Ba3	4f	0.3333	0.6667	0.1853(3)	1
Ba4	2b	0	0	0.25	1
Ti1	4f	0.3333	0.6667	0.0512(8)	1
Ti2	4f	0.6667	0.3333	0.2079(6)	1
O1	4f	0.3333	0.6667	-0.003(2)	1
O2	12k	0.620(6)	0.810(3)	0.0755(7)	1
O3	12k	0.349(7)	0.175(4)	0.1669(8)	1
O4	6h	0.51(5)	0.019(8)	0.25	1

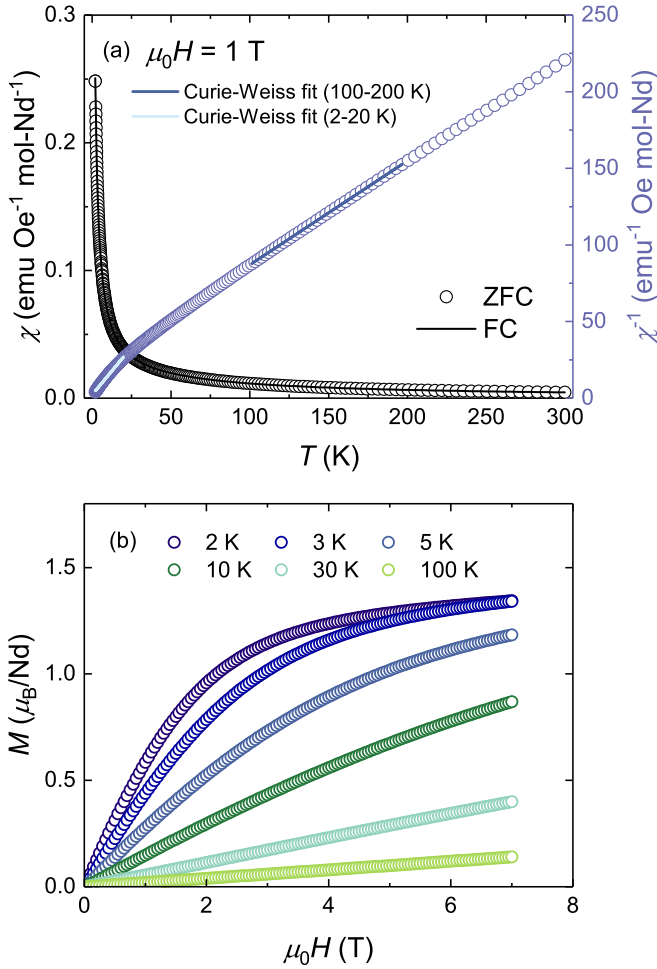


FIG. 3. (a) The temperature dependence of dc magnetic susceptibility and its inverse of $\text{Ba}_6\text{Nd}_2\text{Ti}_4\text{O}_{17}$ at $\mu_0 H = 1$ T measured with ZFC and FC. The solid lines are CW fits in 2–10 K and 100–300 K respectively. (b) The isothermal magnetization at different temperatures down to 2 K.

value $3.62 \mu_B$, and a CW temperature $\Theta_{\text{CW,H}} = -28.1(1)$ K, suggesting antiferromagnetic coupling of Nd^{3+} moments. The susceptibility deviates from CW behavior as the temperature drops below 30 K, but becomes CW again at low temperatures. A CW fit over the range 2–20 K yields $\Theta_{\text{CW,L}} = -1.8$ K.

The strength of the exchange interaction J_{ex} between nearest-neighbor Nd^{3+} spins can be roughly estimated from the mean-field approximation $J_{\text{ex}} = 3k_B \Theta_{\text{CW,L}} / (zJ_{\text{eff}}(J_{\text{eff}} + 1)) \approx 1.2$ K, where $z = 6$ is the number of nearest-neighbor Nd ions and $J_{\text{eff}} = 1/2$ is the effective spin [31]. The effective moment from the low-temperature CW fit is $\mu_{\text{eff,L}} = 2.54 \mu_B$, considerably less than the Hund's-rules value.

The field dependence of the isothermal magnetization $M(H)$ up to 7 T at several temperatures is shown in Fig. 3(b). At 2 K $M(H)$ exhibits a nonlinear field dependence above 1 T, and tends to saturate above 4 T. The energy scale $\mu_{\text{eff,L}} B$ of a 1 T magnetic field for Nd^{3+} spins at low temperatures is 1.7 K, which is of the same order as J_{ex} estimated above. A rough value of the low-temperature saturation moment is $1.3 \mu_B$, about half the value of $\mu_{\text{eff,L}}$, which is expected

from powder-averaged Ising spins in a polycrystalline sample [32]. The field response of the magnetization becomes linear as the temperature increases up to 100 K as a consequence of the decrease in spin-spin correlation. These results are consistent with previously reported data for polycrystalline $\text{Ba}_6\text{Nd}_2\text{Ti}_4\text{O}_{17}$ [27].

C. Specific heat

The absence of spin ordering or spin freezing is indicated by magnetization data down to 2 K (Sec. III B). To confirm this, and to detect potential magnetic excitations, we performed specific heat measurements on polycrystalline $\text{Ba}_6\text{Nd}_2\text{Ti}_4\text{O}_{17}$ down to 0.4 K.

Figure 4(a) shows the measured specific heat at low temperatures and fields up to 8 T. The lack of any sharp anomaly is consistent with the absence of spin ordering. The field dependence is characteristic of Schottky anomalies (but see below).

The temperature dependences of the specific heat at ZF and 8 T up to 300 K are shown in Fig. 4(b). The data for ZF and 8 T basically overlap for $20 \text{ K} < T < 200 \text{ K}$, indicating the absence of excited-state CEF energy levels in this range. The phonon contribution, shown in Fig. 4(c), was obtained by fitting ZF specific heat (2–200 K) with a combination of two Debye and two Einstein functions

$$C_{\text{ph}} = \sum_i^2 f_{\text{Di}} \left[9R \left(\frac{T}{\theta_{\text{Di}}} \right)^3 \int_0^{\theta_{\text{Di}}/T} \frac{x^4 e^x}{(e^x - 1)^2} dx \right] + \sum_i^2 f_{\text{Ei}} \left[3R \left(\frac{\theta_{\text{Ei}}}{T} \right)^2 \frac{e^{\theta_{\text{Ei}}/T}}{(e^{\theta_{\text{Ei}}/T} - 1)^2} \right]. \quad (1)$$

The weight factors were fixed at the ratios $f_{\text{D1}}:f_{\text{D2}}:f_{\text{E1}}:f_{\text{E2}} = 6:15:2:6$, with a sum of 29 atoms per formula unit [33]. The fitting yields Debye temperatures $\theta_{\text{D1}} = 172$ K, $\theta_{\text{D2}} = 726$ K, and Einstein temperatures $\theta_{\text{E1}} = 82$ K, $\theta_{\text{E2}} = 227$ K.

The temperature dependence of the magnetic specific heat C_{m} , obtained by subtracting C_{ph} [Eq. (1)] from the measured total specific heat, is shown in Fig. 5(a). A peak is observed in C_{m} above 1 T that moves to higher temperatures with increasing field. This is characteristic Schottky-anomaly behavior, and was previously reported for single crystal $\text{Ba}_6\text{Nd}_2\text{Ti}_4\text{O}_{17}$ [27]. However, the two-level Schottky function

$$C_{\text{Sch}} = nR \left(\frac{\Delta}{T} \right)^2 \frac{e^{-\Delta/T}}{(1 + e^{-\Delta/T})^2}, \quad (2)$$

where n is the moment concentration, R is the molar gas constant, and Δ is the energy gap between the two levels [34], does not provide good fits to the data (not shown).

This is attributed to the spatial distribution of spin directions in the polycrystalline sample. The Zeeman energy depends on this direction, resulting in a distribution of energy gaps Δ . A uniform angular distribution of spin directions yields a two-level Schottky specific heat given by

$$C = nR \int_0^{\pi/2} \sin \theta d\theta \left[\frac{e^{-\Delta \cos \theta/T} (\Delta \cos \theta)^2}{(1 + e^{-\Delta \cos \theta/T})^2 T^2} \right]. \quad (3)$$

Fits of Eq. (3) to the C_{m} data, shown by dashed curves in Fig. 5(a), are good for fields ≥ 0.1 T, suggesting a

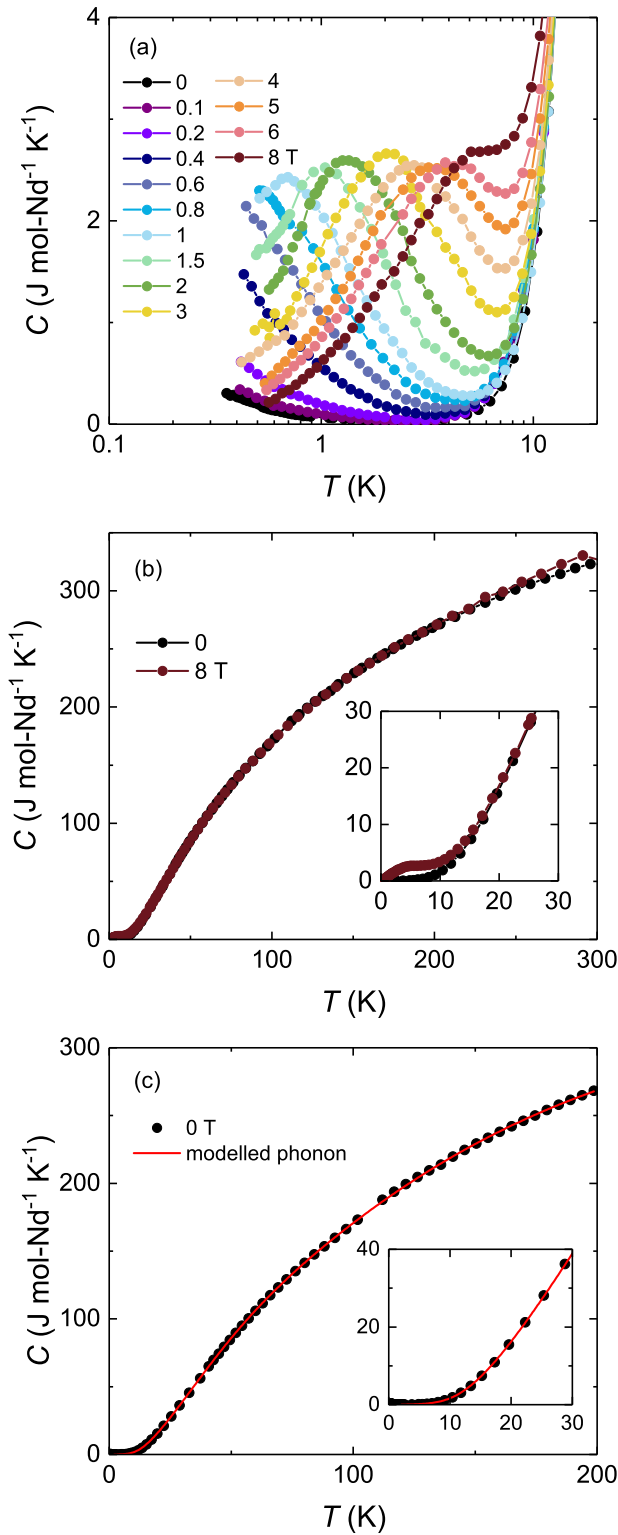


FIG. 4. (a) Low-temperature specific heat of polycrystalline $\text{Ba}_6\text{Nd}_2\text{Ti}_4\text{O}_{17}$ at different applied magnetic fields. (b) Specific heat measured at zero field and 8 T up to 300 K. The inset shows an enlarged view below 30 K. (c) Modeled phonon contribution using Eq. (1). Inset: data below 30 K.

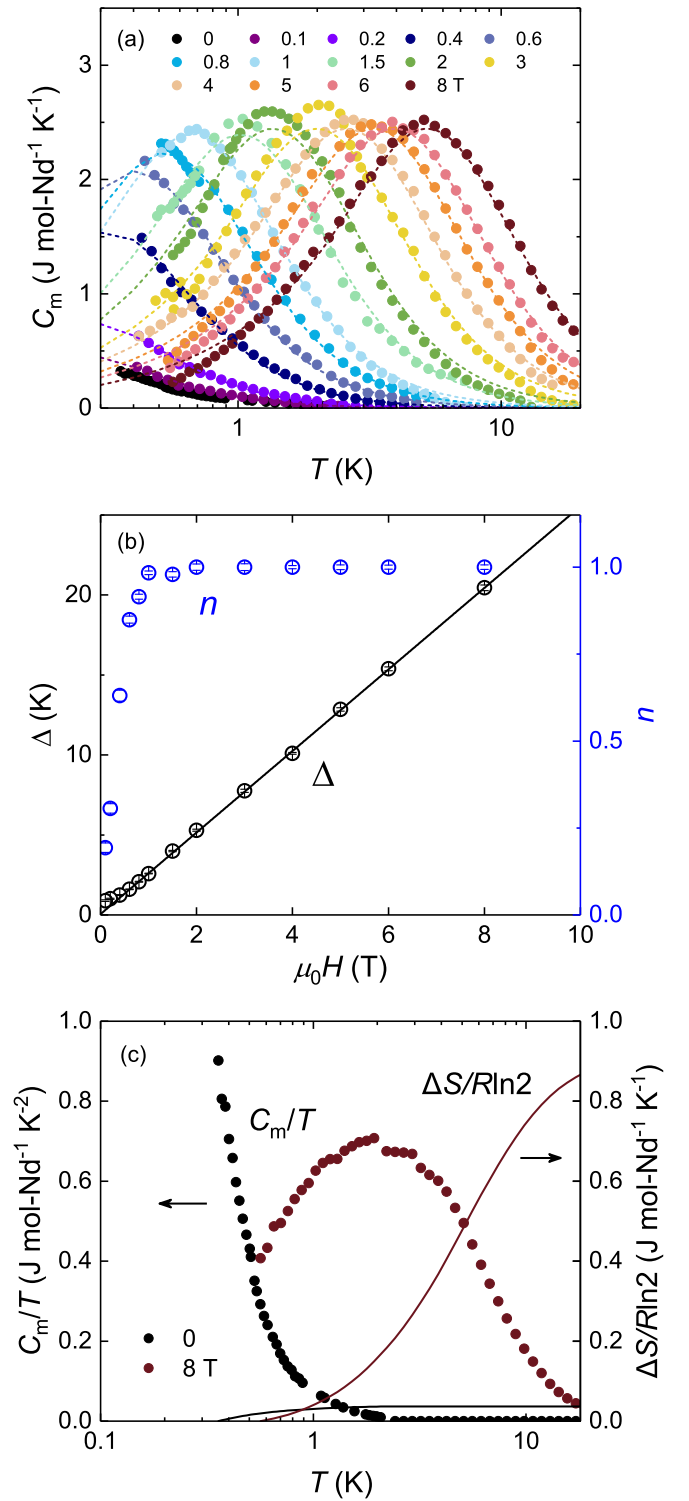


FIG. 5. (a) Magnetic specific heat C_m under different magnetic fields. The dashed lines are a fit to the modified two-energy Schottky model. (b) Field dependence of energy gap Δ and concentration n from fits of Eq. (3) to the data. Solid line: linear fit to $\Delta(H)$ for $\mu_0 H \geq 1$ T. (c) Temperature dependence of magnetic specific heat coefficient C_m/T (points) and calculated entropy (curves) at ZF and 8 T.

ground-state Kramers doublet that is dominant at low temperatures and leads to an effective spin $J_{\text{eff}} = 1/2$.

The field dependences of Δ and n are shown in Fig. 5(b). A linear fit of $\Delta(H)$ is shown for the $n \sim 1$ data, as expected for Zeeman splitting by the field. The fit yields $\mu = 2.56 \mu_B$, essentially the same as $2.54 \mu_B$ from magnetization (Sec. III B). The degeneracy of the ground-state doublet can be lifted by magnetic fields, but at zero and low fields the system cannot be regarded as an assembly of noninteracting two-level ions; a weak field cannot completely lift the degeneracy, resulting in a concentration dependence. Similar behavior has been reported for a number of RE-based oxide insulators [35–37].

Figure 5(c) shows the magnetic specific heat coefficient C_m/T and the corresponding entropy at ZF and 8 T. In 8 T the magnetic entropy at 20 K is nearly $R \ln 2$, the entropy of a spin-1/2 system. The entropy is slightly less than $R \ln 2$ due to the lack of data below ~ 0.6 K. The ZF magnetic entropy only reaches 3% of $R \ln 2$, suggesting considerable residual entropy below 0.4 K.

D. μ SR

μ SR is an ideal technique to probe magnetic order, and is particularly sensitive to slow spin fluctuations [38]. ZF- and LF- μ SR experiments were carried out to further investigate the low-temperature magnetic state of $\text{Ba}_6\text{Nd}_2\text{Ti}_4\text{O}_{17}$.

ZF- μ SR asymmetry spectra at several representative temperatures are shown in Fig. 6(a). Neither oscillations nor a drastic loss of initial asymmetry is observed down to 30 mK, ruling out long- or short-range magnetic order (magnetic freezing) [39]. The lack of polarization recovery to 1/3 indicates μ^+ spin relaxation is dynamic rather than due to static random fields [40,41].

The normalized ZF- μ SR spectra $P(t)$ with background signal subtracted were fit by the function

$$P(t) = f_1 e^{-\lambda_1 t} + (1 - f_1) e^{-\lambda_2 t}, \quad (4)$$

where λ_1 and λ_2 are μ^+ spin relaxation rates and f_1 is the fraction of the first exponential term. f_1 was found to be temperature-independent and was fixed at the average value 0.63.

The temperature dependences of the two ZF rates λ_1 and λ_2 are shown in Fig. 6(b). They exhibit very similar behavior: both increase drastically with decreasing temperature below $T_2 \sim 30$ K, and saturate at $T_1 \sim 4$ K, exhibiting a temperature-independent plateau down to 30 mK. A low-temperature plateau of μ^+ spin relaxation rate is generally regarded as the evidence for persistent spin dynamics and a correlated disordered state [42].

To confirm the dynamical nature of the μ^+ spin relaxation and further investigate the Nd^{3+} spin dynamics, LF- μ SR experiments were carried out. Figure 7(a) shows LF- μ SR spectra measured at 37 mK. The relaxation persists at high applied fields; a longitudinal field of 1 T does not completely “decouple” the μ^+ spin depolarization, i.e., reduce the rate to zero.

If the observed ZF exponential depolarization function originated from a Lorentzian distribution of static fields [43], then the distribution widths $\Delta H_{Li} = \lambda_i / \gamma_\mu$ are ~ 10 mT and ~ 2 mT for $i = 1$ and 2, respectively, where $\gamma_\mu / 2\pi =$

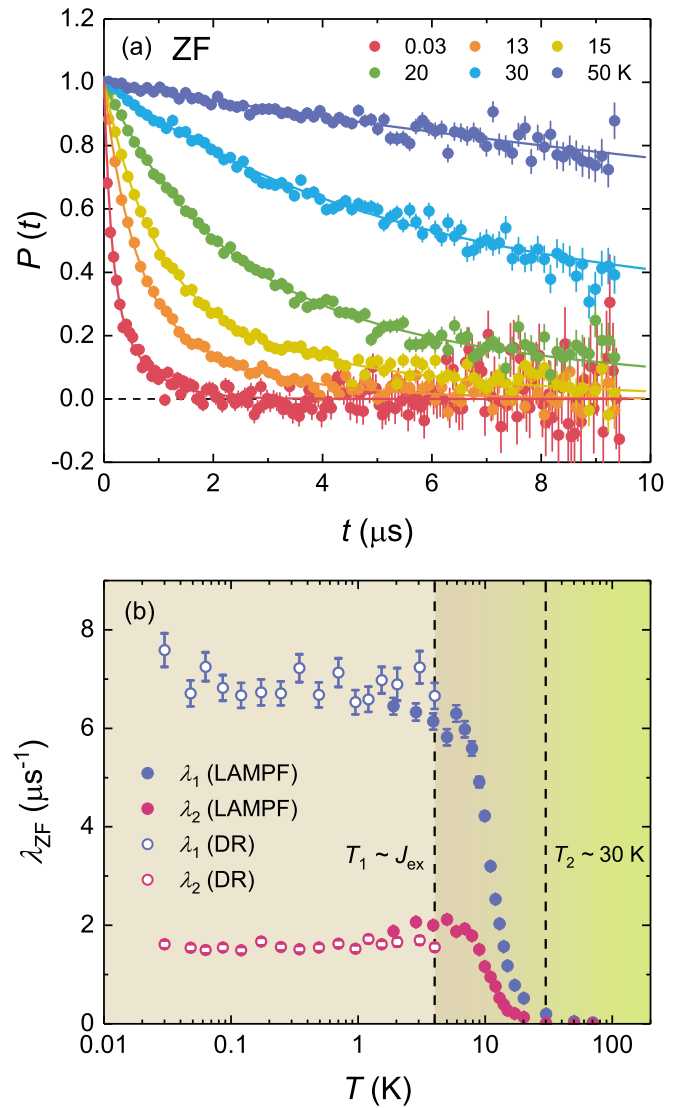


FIG. 6. (a) ZF- μ SR time spectra of polarization at representative temperatures. Solid curves: fits of Eq. (4) to the data. (b) Temperature dependence of ZF- μ SR relaxation rates λ_1 and λ_2 . Open and closed circles: data from the TRIUMF DR and LAMPF spectrometers, respectively. Both rates increase significantly below $T_2 \sim 30$ K, and a plateau is observed below $T_1 \sim 4$ K.

135.54 MHz/T is the gyromagnetic ratio of the muon. An applied field an order of magnitude larger than the static distribution width fully decouples the μ^+ spin depolarization [44], but the maximum field [Fig. 7(a)] of 1 T is two (three) orders of magnitude larger than $\Delta H_{L,1}$ ($\Delta H_{L,2}$) and is still insufficient to decouple the μ^+ spin depolarization. This is strong evidence that dynamic μ^+ spin relaxation persists down to 37 mK in $\text{Ba}_6\text{Nd}_2\text{Ti}_4\text{O}_{17}$.

Representative LF- μ SR spectra measured at 10 K are shown in Fig. 7(b). The relaxation is hardly suppressed by an external longitudinal field of 400 mT, exhibiting a different behavior from that at lower temperatures. The LF- μ SR spectra are also well fitted by Eq. (4) with f_1 fixed at the ZF value 0.63.

The field dependences of λ_1 and λ_2 at four temperatures are shown in Figs. 7(c) and 7(d). The relaxation rate usually

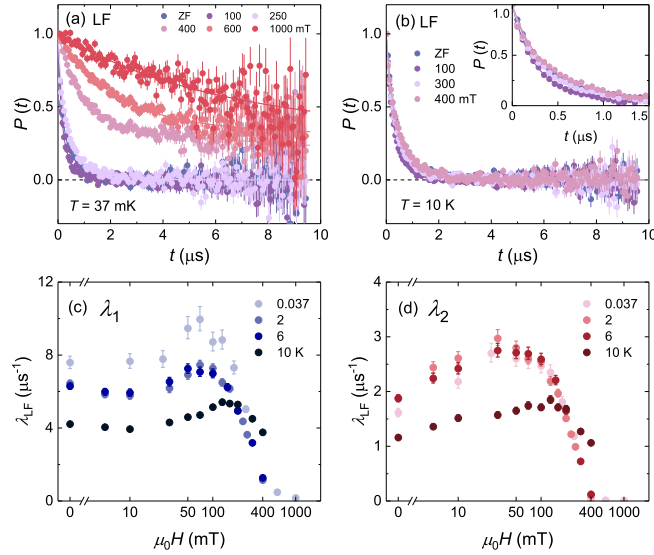


FIG. 7. LF- μ SR asymmetry spectra at representative longitudinal fields at (a) 0.037 K and (b) 10 K. Decoupling is not observed (see text). Inset of (b): early time behavior. (c) and (d) respective field dependences of μ^+ spin relaxation rates λ_1 and λ_2 .

decreases monotonically with increasing external longitudinal field. However, the field dependences of λ_1 and λ_2 both exhibit unusual maxima, which shift to higher fields with increasing temperature up to 10 K. Both rates are quenched rapidly by external longitudinal field above 100 mT below 6 K, but at 10 K they remain comparable to their ZF values even at 400 mT. This unusual field dependence will be discussed in detail below in Sec. IV D.

IV. DISCUSSION

A. Ising anisotropy of Nd^{3+} spins

The electron configuration of Nd^{3+} is $4f^3$. According to Hund's rules, the spin angular momentum $s = 3/2$, the orbital angular momentum $L = 6$, and SOC leads to a total angular momentum $J = 9/2$. The ground state of free Nd^{3+} is tenfold degenerate $^4I_{9/2}$. A point-charge calculation for $\text{Ba}_6\text{Nd}_2\text{Ti}_4\text{O}_{17}$ (Appendix) reveals that the ten $J = 9/2$ states are CEF-split into five Kramers doublets. The specific heat results show that only the ground-state Kramers doublet is occupied below 200 K. Thus the system can be treated as effective spin-1/2 at low temperatures.

The specific heat of single-crystal $\text{Ba}_6\text{Nd}_2\text{Ti}_4\text{O}_{17}$ exhibits perfect two-level Schottky behavior, as expected for spin-1/2 system [27], whereas in the present study the specific heat of a polycrystalline sample can be fit by a modified Schottky model [Eq. (3)]. If the spin directions are assumed to be randomly oriented in the polycrystalline sample, the effective fields experienced by nonparallel spins are reduced and the energy gap of the ground-state doublet split by the magnetic field is distributed.

Random orientation and Ising-like spin anisotropy are both required for a distribution of energy gaps. Ising-like spins basically only experience the z component of the magnetic field. Consequently, the Zeeman energy is highly dependent on the

angle between the spin and the magnetic field, which results in a significant distribution of the energy gap. In contrast, there are a number of polycrystalline materials with effective spin 1/2 [37,45–47] for which the standard two-level Schottky function provides a good fit. For a quantum spin with isotropic exchange the spin coupling is also isotropic.

Ising anisotropy of Nd^{3+} spins in $\text{Ba}_6\text{Nd}_2\text{Ti}_4\text{O}_{17}$ is also supported by the magnetization results. The saturation value of the magnetization at 2 K is $\mu_{\text{sat}} = 1.3 \mu_B$, about half the susceptibility value of $\mu_{\text{eff,L}} = 2.54 \mu_B$, which is a sign of powder-averaged Ising spins in a polycrystalline sample [32]. Ising anisotropy is also consistent with the evidence for Ising-like spins from electron spin resonance measurements on single crystals [27].

The ground-state Kramers doublet created by CEF and SOC is a dipole-octupole (DO) doublet for Nd^{3+} in a triangular lattice with space group of $P6_3/mmc$ or $R\bar{3}m$ [48]. The wave functions of ground-state doublet for $\text{Ba}_6\text{Nd}_2\text{Ti}_4\text{O}_{17}$ from point-charge calculations are given in the Appendix, Table III. They are linear superpositions of the states with $J_z = 3n/2$, where n is an odd integer, indicating the DO doublet nature. Dipolar order together with emergent octupolar order is predicted for DO doublets on triangular lattices with negligible interlayer interactions [48]. However, no dipolar order is observed down to 30 mK in $\text{Ba}_6\text{Nd}_2\text{Ti}_4\text{O}_{17}$. A possible reason is that the exchange interaction between Nd^{3+} spins with interlayer distance d_1 cannot be ignored.

B. Muon stopping sites

The fitting function for μ SR asymmetry spectra [Eq. (4)] includes two exponential terms. The fractions of these terms are nearly temperature-independent, which is usually a sign for signals from distinct μ^+ stopping sites [49], the fitting function for LF- μ SR and ZF- μ SR is the same, and the relaxation rates show similar temperature and field dependences. These properties are consistent with their attribution to two inequivalent μ^+ stopping sites.

μ^+ sites generally maximize the number of near-neighbor O^{2-} ions. In the $\text{Ba}_6\text{Nd}_2\text{Ti}_4\text{O}_{17}$ structure the two sites S1 and S2 shown in Fig. 1(c) satisfy this criteria. S1 is located between two Nd^{3+} layers and close to TiO_4 tetrahedra or Ti_2O_9 dimers, and S2 is in the Nd layer and close to NdO_6 octahedra. The ratio of the two kinds of O–O bonds is 1.38, comparable to the ratio of the two fractions of exponential terms in the asymmetry spectra (≈ 1.7). λ_1 is several times larger than λ_2 , which may be related to the strength of the local magnetic field at each μ^+ site.

The evidence for these stopping sites is of course very qualitative. Density functional theory calculations were unsuccessful because of the large number of atoms in the unit cell. Precise knowledge of the sites is, however, not essential to the present work.

C. Spin dynamics

a. Frustration vs Nd^{3+} distances. Frustration and long distances between magnetic ions can both be involved in suppression of magnetic freezing. In Table II we list ion spacing and frustration parameters for some Nd-based

TABLE II. Structural and magnetic properties of some Nd-based triangular-lattice antiferromagnets.

Compound	d_{inter} (Å)	d_{intra} (Å)	θ_{CW} (K)	f
Ba ₆ Nd ₂ Ti ₄ O ₁₇	7.40	5.99	-1.8	> 60
NdT _{a7} O ₁₉ ^a	9.97	6.62	-0.46	> 11.5
CsNdSe ₂ ^b		-4.35	-0.66 ($H \parallel c$)	> 16.5
NdZnAl ₁₁ O ₁₉ ^c	11.43	5.59	-1.23	> 0.6
KNdSe ₂ ^d	7.60	4.31	-1.9 ($H \parallel c$)	> 4.7

^aReference [22].

^bReference [50].

^cReference [51].

^dReference [52].

triangular lattices for comparison. None of them exhibit magnetic ordering at low temperatures. Although the Nd-Nd distance within the triangular layer is about 6 Å for Ba₆Nd₂Ti₄O₁₇, the frustration parameter $f > 60$, indicating a significant suppression of magnetic ordering. Therefore, the magnetic disorder is not due to the isolation of magnetic ions.

b. Temperature dependence. Two characteristic temperatures $T_1 \sim 4$ K and $T_2 \sim 30$ K are observed in ZF- μ SR measurements [Fig. 6(b)]. The μ^+ spin relaxation rates rise rapidly below $T_2 \sim 30$ K, and exhibit a plateau below $T_1 \sim 4$ K. $k_B T_1$ is of the order of the exchange interaction $J_{\text{ex}} \sim 1.2$ K, suggesting the onset of spin correlation. The low-temperature plateau of $\lambda_{1,2}$ indicates the spin fluctuation no longer slows down as temperature drops, and signals a disordered magnetic ground state with persistent dynamics. This is further confirmed by LF- μ SR measurements.

It is informative to compare the behavior of $\lambda_{1,2}$ at T_2 with the estimated μ^+ spin relaxation rate λ_∞ for a local-moment paramagnet in the high-temperature limit $T \rightarrow \infty$. λ_∞ is temperature independent and approximately $2(\gamma_\mu H_{\text{rms}})^2/\nu$ [53], where H_{rms} is the rms field at a μ^+ site and the exchange fluctuation rate $\nu \approx \sqrt{z} J_{\text{ex}} S/\hbar$; z and S are the local-moment coordination number and spin, and J_{ex} is the exchange energy.

With $z = 6$, and using the low-temperature $J_{\text{ex}} = 1.2$ K (Sec. III B) and $S = J_{\text{eff}} = 1/2$, we find $\nu \approx 1.9 \times 10^{11}$ s⁻¹. Using the high-temperature Nd moment $3.43 \mu_B$, $\mu_0 H_{\text{rms}} = 103$ mT assuming a dipolar field and uncorrelated fluctuations. This yields $\lambda_\infty \approx 0.13 \mu\text{s}^{-1}$, much less than the observed rates at 10 K. It would be an order of magnitude smaller if $\Theta_{\text{CW,H}}$ were used to evaluate the exchange instead of $\Theta_{\text{CW,L}}$.

The values and strong temperature dependences of the observed rates $\lambda_{1,2}$ below T_2 [Fig. 6(b)] do not characterize the high-temperature paramagnetic state. The onset of Nd³⁺ spin correlations slows their fluctuations with decreasing temperature, thus increasing $\lambda(T)$ so that it becomes observable at lower temperatures.

D. Field dependence of μ^+ spin relaxation rates

The local magnetic field in Ba₆Nd₂Ti₄O₁₇ at low temperatures has been shown to be dynamical by LF- μ SR measurements, but the field dependence of μ^+ spin relaxation rates shows an unusual maximum. Level-crossing resonance (LCR) can lead to a resonance peak in the field dependence

of μ^+ spin relaxation rates at $B_{\text{res}} = \omega_Q/\gamma_\mu$, where ω_Q is the quadrupolar frequency [54]. LCR occurs when the μ^+ Zeeman frequency in an external field is equal to the quadrupolar frequency of nuclei with spins larger than 1/2 [55]. A resonance peak due to LCR centered at ~ 8 mT was previously reported for Cu metal [54], due to a μ^+ -induced electric field gradient (EFG) at ^{63,65}Cu sites.

A LCR peak might be expected in Ba₆Nd₂Ti₄O₁₇. The quadrupole moments of Ba, Nd, Ti, and Cu nuclei are of the same order (0.1 barn) as Cu, and ω_Q is proportional to the quadrupole moment [44]. The extrema of the LF μ^+ relaxation rates Ba₆Nd₂Ti₄O₁₇ are observed around 100 mT, but the higher field may reflect the intrinsic EFG at the noncubic lattice sites. Thus LCR cannot be excluded. NMR/NQR measurements in Ba₆Nd₂Ti₄O₁₇ are needed to clarify this issue.

For the case of random fluctuations originating from localized and uncorrelated spins, the spin dynamic autocorrelation function generally takes an exponential form, $S(t) \sim e^{-\nu t}$, where ν is the field fluctuation rate. Then the μ^+ spin relaxation rate can be expressed by the Redfield formula [55]

$$\lambda(H) = \frac{2(\gamma_\mu \Delta H_{\text{loc}})^2 \nu}{\nu^2 + (\gamma_\mu H_0)^2} \quad (5)$$

in the fast fluctuation limit ($\gamma_\mu \Delta H_{\text{loc}} \ll \nu$), where ΔH_{loc} is the Gaussian distribution width of local magnetic fields, ν is the field fluctuation rate, and H_0 is the applied longitudinal magnetic field. $\lambda(H)$ described by the Redfield formula monotonically decreases as the external field is increased when ΔH_{loc} and ν are nearly unchanged, which is inconsistent with the observed field dependence of $\lambda_{1,2}$ here.

We recall that the energy scale of exchange interactions is about 1 K for Ba₆Nd₂Ti₄O₁₇. At $T = 10$ K, thermal fluctuations are relatively strong, and the exchange interactions are negligible. The extremum of $\lambda_{1,2}$ persists at temperature up to 10 K, suggesting it does not result from exchange interactions or spin correlation. The extremum of $\lambda_{1,2}$ may be due to the change in the distribution width of local fields ΔH_{loc} . Since the field coupling of Ising spins are highly anisotropic and the sample is polycrystalline, a field dependence of ΔH_{loc} may be significant to drive $\lambda(H)$ no longer monotonic.

Both λ_1 and λ_2 remain a sizable value at 10 K under 400 mT. The field independence of $\lambda_{1,2}$ is reminiscent of a similar result in YbZnGaO₄ [56], which was attributed to rapidly fluctuating local spins. As noted above, however, in the high-temperature limit the Nd³⁺ spin fluctuation rate ν is essentially the Nd spin precession frequency in the exchange field, so that λ is temperature-independent at a low value.

V. CONCLUSIONS

Polycrystalline antiferromagnetic Ba₆Nd₂Ti₄O₁₇ with an essentially disorder-free triangular lattice has been synthesized and studied. The absence of long-range magnetic order and spin freezing is confirmed down to 30 mK by ZF- μ SR measurements. The negative CW temperature $\Theta_{\text{CW}} = -1.8$ K from magnetic susceptibility measurements indicates an antiferromagnetic exchange interaction of Nd³⁺ spins. The low-temperature magnetic specific heat is well fitted by a modified two-level Schottky model, suggesting the system has an effective Ising spin $J_{\text{eff}} = 1/2$ at low temperatures due

TABLE III. Calculated eigenvalues and eigenvectors of CEF energy levels for $\text{Ba}_6\text{Nd}_2\text{Ti}_4\text{O}_{17}$.

E (meV)	$ \frac{9}{2}\rangle$	$ \frac{7}{2}\rangle$	$ \frac{5}{2}\rangle$	$ \frac{3}{2}\rangle$	$ \frac{1}{2}\rangle$	$ \frac{1}{2}\rangle$	$ \frac{3}{2}\rangle$	$ \frac{5}{2}\rangle$	$ \frac{7}{2}\rangle$	$ \frac{9}{2}\rangle$
0	0.753	0	0	-0.655	0	0	0.025	0	0	-0.061
0	0.061	0	0	0.025	0	0	0.655	0	0	0.753
0.401	0	-0.91	0.04	0	0.291	0.046	0	-0.253	0.142	0
0.401	0	-0.142	-0.253	0	0.046	-0.291	0	-0.04	-0.91	0
12.366	0	0.095	-0.822	0	-0.122	0.209	0	-0.481	0.162	0
12.366	0	-0.162	-0.481	0	0.209	0.122	0	0.822	0.095	0
72.528	0.656	0	0	0.749	0	0	-0.098	0	0	0.007
72.528	-0.007	0	0	-0.098	0	0	-0.749	0	0	0.656
76.633	0	-0.059	0.165	0	-0.16	0.911	0	0.029	-0.337	0
76.633	0	-0.337	-0.029	0	-0.911	-0.16	0	0.165	0.059	0

to a ground-state Kramers doublet. Ising spin anisotropy is also supported by the effective moment from magnetization measurements.

The low-temperature plateau of μ^+ spin relaxation rates in ZF- μ SR indicates a quantum disordered ground state, and LF- μ SR measurements give further evidence for persistent spin dynamics for temperatures down to 37 mK. These results are consistent with a QSL picture, where the spins remain disordered and fluctuate strongly even at zero temperature [22,42,57,58].

Intriguing behavior has been observed in a triangular-lattice antiferromagnet with effective Ising spin 1/2. It provides an excellent example of a system that remains magnetically disordered down to $\sim|\Theta_{\text{CW}}|/60$ with persistent spin dynamics. However, more experiments are needed, especially on single crystals, to characterize the spin excitations at low temperatures and to confirm the ground state.

ACKNOWLEDGMENTS

We are grateful to G. D. Morris, B. Hitti, and D. Arsenau of the TRIUMF CMMS for assistance during the experiments.

We thank G. Chen, Y. Wan, and Y. Wang for discussions. This research was funded by the National Key Research and Development Program of China, No. 2022YFA1402203, the National Natural Science Foundations of China, No. 12174065, and the Shanghai Municipal Science and Technology Major Project (Grant No. 2019SHZDZX01). Research at CSU-Fresno was supported by NSF DMR-1905636.

APPENDIX: POINT-CHARGE CALCULATIONS

Eigenvalues and eigenvectors of CEF energy levels in $\text{Ba}_6\text{Nd}_2\text{Ti}_4\text{O}_{17}$ were calculated based on the point-charge approximation, using the software package PYCRYSTALFIELD [59]. The wave functions are superpositions of $|J_z\rangle$ eigenfunctions, with coefficients shown in Table III. The CEF energy levels are five Kramers doublets. We note that the calculated energy values are not reliable due to the point-charge approximation. In particular, the 8 T magnetic specific heat $C_m(T)$ (Fig. 5) is not consistent with a first excited CEF state energy of 0.401 meV = 4.65 K. The CEF level energies can only be determined from additional measurements, e.g., inelastic neutron scattering.

- [1] L. Balents, Spin liquids in frustrated magnets, *Nature (London)* **464**, 199 (2010).
- [2] P. W. Anderson, The resonating valence bond state in La_2CuO_4 and superconductivity, *Science* **235**, 1196 (1987).
- [3] X.-G. Wen, Quantum orders and symmetric spin liquids, *Phys. Rev. B* **65**, 165113 (2002).
- [4] H. Takagi, T. Takayama, G. Jackeli, G. Khaliullin, and S. E. Nagler, Concept and realization of Kitaev quantum spin liquids, *Nat. Rev. Phys.* **1**, 264 (2019).
- [5] X. G. Wen, Effective Lagrangian for holes in the spin-liquid state, *Phys. Rev. B* **39**, 7223 (1989).
- [6] X. G. Wen, Mean-field theory of spin-liquid states with finite energy gap and topological orders, *Phys. Rev. B* **44**, 2664 (1991).
- [7] P. Anderson, Resonating valence bonds: A new kind of insulator? *Mater. Res. Bull.* **8**, 153 (1973).
- [8] D. A. Huse and V. Elser, Simple variational wave functions for two-dimensional Heisenberg spin- $\frac{1}{2}$ antiferromagnets, *Phys. Rev. Lett.* **60**, 2531 (1988).
- [9] Y. Iqbal, W.-J. Hu, R. Thomale, D. Poilblanc, and F. Becca, Spin liquid nature in the Heisenberg $J_1 - J_2$ triangular antiferromagnet, *Phys. Rev. B* **93**, 144411 (2016).
- [10] Z. Zhu and S. R. White, Spin liquid phase of the $S = \frac{1}{2}J_1 - J_2$ Heisenberg model on the triangular lattice, *Phys. Rev. B* **92**, 041105(R) (2015).
- [11] Q. Luo, S. Hu, B. Xi, J. Zhao, and X. Wang, Ground-state phase diagram of an anisotropic spin- $\frac{1}{2}$ model on the triangular lattice, *Phys. Rev. B* **95**, 165110 (2017).
- [12] O. I. Motrunich, Variational study of triangular lattice spin- $\frac{1}{2}$ model with ring exchanges and spin liquid state in $\kappa\text{-(ET)}_2\text{Cu}_2(\text{CN})_3$, *Phys. Rev. B* **72**, 045105 (2005).
- [13] D. Yamamoto, G. Marmorini, and I. Danshita, Quantum phase diagram of the triangular-lattice XXZ model in a magnetic field, *Phys. Rev. Lett.* **112**, 127203 (2014).
- [14] Y.-D. Li, X. Wang, and G. Chen, Anisotropic spin model of strong spin-orbit-coupled triangular antiferromagnets, *Phys. Rev. B* **94**, 035107 (2016).

- [15] W. Witczak-Krempa, G. Chen, Y. B. Kim, and L. Balents, Correlated quantum phenomena in the strong spin-orbit regime, *Annu. Rev. Condens. Matter Phys.* **5**, 57 (2014).
- [16] Y. Li, H. Liao, Z. Zhang, S. Li, F. Jin, L. Ling, L. Zhang, Y. Zou, L. Pi, Z. Yang, J. Wang, Z. Wu, and Q. Zhang, Gapless quantum spin liquid ground state in the two-dimensional spin- $\frac{1}{2}$ triangular antiferromagnet YbMgGaO_4 , *Sci. Rep.* **5**, 16419 (2015).
- [17] Y. Shen, Y.-D. Li, H. Wo, Y. Li, S. Shen, B. Pan, Q. Wang, H. C. Walker, P. Steffens, M. Boehm, Y. Hao, D. L. Quintero-Castro, L. W. Harriger, M. D. Frontzek, L. Hao, S. Meng, Q. Zhang, G. Chen, and J. Zhao, Evidence for a spinon Fermi surface in a triangular-lattice quantum-spin-liquid candidate, *Nature (London)* **540**, 559 (2016).
- [18] Y.-D. Li, Y.-M. Lu, and G. Chen, Spinon Fermi surface $U(1)$ spin liquid in the spin-orbit-coupled triangular-lattice Mott insulator YbMgGaO_4 , *Phys. Rev. B* **96**, 054445 (2017).
- [19] L. Ding, P. Manuel, S. Bachus, F. Größler, P. Gegenwart, J. Singleton, R. D. Johnson, H. C. Walker, D. T. Adroja, A. D. Hillier, and A. A. Tsirlin, Gapless spin-liquid state in the structurally disorder-free triangular antiferromagnet NaYbO_2 , *Phys. Rev. B* **100**, 144432 (2019).
- [20] M. Baenitz, P. Schlender, J. Sichelschmidt, Y. A. Onyikienko, Z. Zangeneh, K. M. Ranjith, R. Sarkar, L. Hozoi, H. C. Walker, J.-C. Orain, H. Yasuoka, J. van den Brink, H. H. Klauss, D. S. Inosov, and T. Doert, NaYbS_2 : A planar spin- $\frac{1}{2}$ triangular-lattice magnet and putative spin liquid, *Phys. Rev. B* **98**, 220409(R) (2018).
- [21] Z. Zhu, B. Pan, L. Nie, J. Ni, Y. Yang, C. Chen, C. Jiang, Y. Huang, E. Cheng, Y. Yu, J. Miao, A. D. Hillier, X. Chen, T. Wu, Y. Zhou, S. Li, and L. Shu, Fluctuating magnetic droplets immersed in a sea of quantum spin liquid, *The Innovation* **4**, 100459 (2023).
- [22] T. Arh, B. Sana, M. Pregelj, P. Khuntia, Z. Jagličić, M. D. Le, P. K. Biswas, P. Manuel, L. Mangin-Thro, A. Ozarowski, and A. Zorko, The Ising triangular-lattice antiferromagnet neodymium heptatantalate as a quantum spin liquid candidate, *Nat. Mater.* **21**, 416 (2022).
- [23] J. Khatua, B. Sana, A. Zorko, M. Gomilšek, K. Sethupathi, M. R. Rao, M. Baenitz, B. Schmidt, and P. Khuntia, Experimental signatures of quantum and topological states in frustrated magnetism, *Phys. Rep.* **1041**, 1 (2023).
- [24] G. H. Wannier, Antiferromagnetism. The triangular Ising net, *Phys. Rev.* **79**, 357 (1950).
- [25] P. Fazekas and P. W. Anderson, On the ground state properties of the anisotropic triangular antiferromagnet, *Philos. Mag.* **30**, 423 (1974).
- [26] R. Moessner and S. L. Sondhi, Ising models of quantum frustration, *Phys. Rev. B* **63**, 224401 (2001).
- [27] F. Song, A. Liu, Q. Chen, J. Zhou, J. Li, W. Tong, S. Wang, Y. Wang, H. Lu, S. Yuan, H. Guo, and Z. Tian, $\text{Ba}_6\text{R}_2\text{Ti}_4\text{O}_{17}$ ($\text{RE} = \text{Nd, Sm, Gd, Dy-Yb}$): A family of rare-earth-based layered triangular lattice magnets, *Inorg. Chem.* **63**, 5831 (2024).
- [28] X. Kuang, X. Jing, C.-K. Loong, E. E. Lachowski, J. M. S. Skakle, and A. R. West, A new hexagonal 12-layer perovskite-related structure: $\text{Ba}_6\text{R}_2\text{Ti}_4\text{O}_{17}$ ($\text{R} = \text{Nd and Y}$), *Chem. Mater.* **14**, 4359 (2002).
- [29] J. Rodriguez-Carvajal, *FULLPROF-A Program for Rietveld Profile Matching and Integrated Intensities Refinement of X-Ray and/or Neutron Data* (CEA-Saclay, France, 2000).
- [30] A. Suter and B. Wojek, MUSRFIT: A free platform-independent framework for μSR data analysis, *Phys. Procedia* **30**, 69 (2012).
- [31] J. E. Greedan, Geometrically frustrated magnetic materials, *J. Mater. Chem.* **11**, 37 (2001).
- [32] S. T. Bramwell, M. N. Field, M. J. Harris, and I. P. Parkin, Bulk magnetization of the heavy rare earth titanate pyrochlores - a series of model frustrated magnets, *J. Phys.: Condens. Matter* **12**, 483 (2000).
- [33] The weight factors are often not the formula-unit values; see, e.g., Ref. [58].
- [34] A. Tari, *The Specific Heat of Matter at Low Temperatures* (Imperial College Press, London, 2003).
- [35] C. Y. Jiang, Y. X. Yang, Y. X. Gao, Z. T. Wan, Z. H. Zhu, T. Shiroka, C. S. Chen, Q. Wu, X. Li, J. C. Jiao, K. W. Chen, Y. Bao, Z. M. Tian, and L. Shu, Spin excitations in the quantum dipolar magnet $\text{Yb}(\text{BaBO}_3)_3$, *Phys. Rev. B* **106**, 014409 (2022).
- [36] E. Lhotel, L. Mangin-Thro, E. Ressouche, P. Steffens, E. Bichaud, G. Knebel, J.-P. Brison, C. Marin, S. Raymond, and M. E. Zhitomirsky, Spin dynamics of the quantum dipolar magnet $\text{Yb}_3\text{Ga}_5\text{O}_{12}$ in an external field, *Phys. Rev. B* **104**, 024427 (2021).
- [37] J. Khatua, M. Pregelj, A. Elghandour, Z. Jagličić, R. Klingeler, A. Zorko, and P. Khuntia, Magnetic properties of the triangular-lattice antiferromagnets $\text{Ba}_3\text{RB}_9\text{O}_{18}$ ($\text{R} = \text{Yb, Er}$), *Phys. Rev. B* **106**, 104408 (2022).
- [38] A. D. Hillier, S. J. Blundell, I. McKenzie, I. Umegaki, L. Shu, J. A. Wright, T. Prokscha, F. Bert, K. Shimomura, A. Berlie, H. Alberto, and I. Watanabe, Muon spin spectroscopy, *Nat. Rev. Methods Primers* **2**, 4 (2022).
- [39] X. G. Zheng, H. Kubozono, K. Nishiyama, W. Higemoto, T. Kawae, A. Koda, and C. N. Xu, Coexistence of long-range order and spin fluctuation in geometrically frustrated clinoatacamite $\text{Cu}_2\text{Cl}(\text{OH})_3$, *Phys. Rev. Lett.* **95**, 057201 (2005).
- [40] R. Kubo and T. Toyabe, A stochastic model for low field resonance and relaxation, in *Magnetic Resonance and Relaxation*, edited by R. Blinc (North-Holland, Amsterdam, 1967), pp. 810–823.
- [41] R. S. Hayano, Y. J. Uemura, J. Imazato, N. Nishida, T. Yamazaki, and R. Kubo, Zero- and low-field spin relaxation studied by positive muons, *Phys. Rev. B* **20**, 850 (1979).
- [42] L. Clark, G. Sala, D. D. Maharaj, M. B. Stone, K. S. Knight, M. T. F. Telling, X. Wang, X. Xu, J. Kim, Y. Li, S.-W. Cheong, and B. D. Gaulin, Two-dimensional spin liquid behaviour in the triangular-honeycomb antiferromagnet TbInO_3 , *Nat. Phys.* **15**, 262 (2019).
- [43] Y. J. Uemura, T. Yamazaki, D. R. Harshman, M. Senba, and E. J. Ansaldo, Muon-spin relaxation in AuFe and CuMn spin glasses, *Phys. Rev. B* **31**, 546 (1985).
- [44] A. Yaouanc and P. D. de Réotier, *Muon Spin Rotation, Relaxation, and Resonance: Applications to Condensed Matter* (Oxford University Press, Oxford, UK, 2011).
- [45] J. Khatua, S. Bhattacharya, A. M. Strydom, A. Zorko, J. S. Lord, A. Ozarowski, E. Kermarrec, and P. Khuntia, Magnetic properties and spin dynamics in the spin-orbit driven $J_{\text{eff}} = \frac{1}{2}$ triangular lattice antiferromagnet $\text{Ba}_6\text{Yb}_2\text{Ti}_4\text{O}_{17}$, *Phys. Rev. B* **109**, 024427 (2024).
- [46] J. Khatua, S. Bhattacharya, Q. P. Ding, S. Vrtnik, A. M. Strydom, N. P. Butch, H. Luetkens, E. Kermarrec, M. S. R. Rao, A. Zorko, Y. Furukawa, and P. Khuntia, Spin liquid state

- in a rare-earth hyperkagome lattice, *Phys. Rev. B* **106**, 104404 (2022).
- [47] M. Ennis, R. Bag, C. Liu, S. E. Dissanayake, A. I. Kolesnikov, L. Balents, and S. Haravifard, Realization of two-sublattice exchange physics in the triangular lattice compound $\text{Ba}_3\text{Er}(\text{BO}_3)_3$, *Commun. Phys.* **7**, 37 (2024).
- [48] Y.-D. Li, X. Wang, and G. Chen, Hidden multipolar orders of dipole-octupole doublets on a triangular lattice, *Phys. Rev. B* **94**, 201114(R) (2016).
- [49] Z. Zhu and L. Shu, Muon spin relaxation studies on quantum spin liquid candidates, *Prog. Phys.* **40**, 143 (2020).
- [50] J. Xing, S. Mu, E. S. Choi, and R. Jin, Candidate spin-liquid ground state in CsNdSe_2 with an effective spin- $\frac{1}{2}$ triangular lattice, *Commun. Mater.* **5**, 45 (2024).
- [51] M. Ashtar, M. A. Marwat, Y. X. Gao, Z. T. Zhang, L. Pi, S. L. Yuan, and Z. M. Tian, $\text{REZnAl}_{11}\text{O}_{19}$ (RE = Pr, Nd, Sm-Tb): A new family of ideal 2D triangular lattice frustrated magnets, *J. Mater. Chem. C* **7**, 10073 (2019).
- [52] L. D. Sanjeewa, J. Xing, K. M. Taddei, and A. S. Sefat, Synthesis, crystal structure and magnetic properties of KLnSe_2 (Ln = La, Ce, Pr, Nd) structures: A family of 2D triangular lattice frustrated magnets, *J. Solid State Chem.* **308**, 122917 (2022).
- [53] Y. J. Uemura, A. Keren, K. Kojima, L. P. Le, G. M. Luke, W. D. Wu, Y. Ajiro, T. Asano, Y. Kuriyama, M. Mekata, H. Kikuchi, and K. Kakurai, Spin fluctuations in frustrated kagomé lattice system $\text{SrCr}_8\text{Ga}_4\text{O}_{19}$ studied by muon spin relaxation, *Phys. Rev. Lett.* **73**, 3306 (1994).
- [54] S. R. Kreitzman, J. H. Brewer, D. R. Harshman, R. Keitel, D. L. Williams, K. M. Crowe, and E. J. Ansaldo, Longitudinal-field μ^+ spin relaxation via quadrupolar level-crossing resonance in Cu at 20 K, *Phys. Rev. Lett.* **56**, 181 (1986).
- [55] S. J. Blundell, R. D. Renzi, T. Lancaster, and F. L. Pratt, *Muon Spectroscopy: An Introduction* (Oxford University Press, Oxford, UK, 2022).
- [56] F. L. Pratt, F. Lang, W. Steinhardt, S. Haravifard, and S. J. Blundell, Spin dynamics, entanglement, and the nature of the spin liquid state in YbZnGaO_4 , *Phys. Rev. B* **106**, L060401 (2022).
- [57] Y. Li, D. Adroja, P. K. Biswas, P. J. Baker, Q. Zhang, J. Liu, A. A. Tsirlin, P. Gegenwart, and Q. Zhang, Muon spin relaxation evidence for the U(1) quantum spin-liquid ground state in the triangular antiferromagnet YbMgGaO_4 , *Phys. Rev. Lett.* **117**, 097201 (2016).
- [58] S. Kundu, A. Shahee, A. Chakraborty, K. M. Ranjith, B. Koo, J. Sichelschmidt, M. T. F. Telling, P. K. Biswas, M. Baenitz, I. Dasgupta, S. Pujari, and A. V. Mahajan, Gapless quantum spin liquid in the triangular system $\text{Sr}_3\text{CuSb}_2\text{O}_9$, *Phys. Rev. Lett.* **125**, 267202 (2020).
- [59] A. Scheie, PyCrystalField: software for calculation, analysis and fitting of crystal electric field Hamiltonians, *J. Appl. Cryst.* **54**, 356 (2021).